A CONTINUATION METHOD FOR COMPUTING GLOBAL ISOCHRONS

HINKE M. OSINGA* AND JEFF MOEHLIS†

Abstract. Isochrons are foliations of phase space that extend the notion of phase of a stable periodic orbit to the basin of attraction of this periodic orbit. Each point in the basin of attraction lies on only one isochron and two points on the same isochron converge to the periodic orbit with the same phase. These properties allow one to define so-called phase models that reduce the dimension of an oscillating system. Global isochrons, that is, isochrons extended into the full basin of attraction rather than just a neighborhood of the periodic orbit, can typically only be approximated numerically. Unfortunately, their computation is rather difficult, particularly for systems with multiple time scales. We present a novel method for computing isochrons via the continuation of a two-point boundary value problem. We view the isochron associated with a particular phase point γ on the periodic orbit as the Poincaré section of the time-T return map that has γ as its fixed point; here, the time T is the period of the periodic orbit. The boundary value problem set-up uses the orbit segment that defines the periodic orbit starting at γ as the first known solution on the isochron; other solutions are found by continuation along the linear approximation of the isochron in a prespecified small neighborhood of the periodic orbit. This means that the computational error is fully controlled by the accuracy settings of the boundary value solver and the maximal distance along the linear approximation. This method can easily be implemented for two-dimensional systems, and we are able to compute global isochrons of planar slow-fast systems in unprecedented detail. We show how complicated the structure of isochrons can be already for such low-dimensional systems and discuss how the isochrons determine the phase sensitivity of the system.

Key words. isochron, phase response curve, Hodgkin-Huxley, two-point boundary value problem, continuation method

AMS subject classifications. 37C10, 65P99, 37N25

1. Introduction.

Many biological systems produce rhythmic oscillations that are self-sustained, with an internal source of energy being transformed into oscillations of chemical concentrations and electrical and mechanical properties. Such biological oscillators have a long, successful history of being modeled using ordinary differential equations [26, 28]. A prototypical example of a biological oscillator is the stable periodically firing action potential generated by the giant axon of a squid for a range of constant bias currents [25]. This behavior was famously modeled by Hodgkin and Huxley [25] using a four-dimensional system of coupled nonlinear ordinary differential equations, representing the voltage difference across a neural membrane and three gating variables related to ionic flow across the membrane.

A powerful technique for analyzing a biological oscillator is the rigorous reduction to a phase model, with a single variable describing the phase of the oscillation with respect to some reference state; see, for example, [3, 21]. This tremendous reduction in the dimensionality and complexity of a system often retains enough information to gain a useful understanding of its dynamics. Moreover, the analysis of the system is greatly simplified, because phase models tend to depend only on a very small number of parameters [3]. The reduction to a phase model is based on the notion of *isochrons*

*Department of Engineering Mathematics, University of Bristol, Bristol, BS8 1TR, United Kingdom (H.M.Osinga@bristol.ac.uk); research supported by an Advanced Research Fellowship from the Engineering and Physical Sciences Research Council and an IGERT grant from the National Science Foundation.

†Department of Mechanical Engineering, University of California, Santa Barbara, CA 93106, United States of America (moehlis@engineering.ucsb.edu); research supported by the National Science Foundation grant NSF-0547606.

of the oscillator for the system. Isochrons are sets in phase space that correspond to solution trajectories that asymptotically approach a stable periodic orbit Γ (the oscillator) at identical phases. They are defined relative to Γ and make sense only for points in the basin of attraction of Γ. The isochrons give a sense of how long a trajectory spends in different regions of phase space: for example, a trajectory moves slowly through regions of state space where isochrons that are equally spaced in phase lie relatively close to each other.

The concept of an isochron is also important in power electronics. Power generation systems consist of several generating units that operate in parallel. Before a new unit, for example, a wind turbine or solar panel, can be connected to a utility network, one must ensure precise amplitude, frequency and phase conditions. In particular, phase agreement between the voltages of the generator and the power system at the instant of connection is critical because of the electromagnetic transients that follow [20, 42]. Such grid synchronization problems essentially require that the new unit be connected at the precise moment when its state vector is such that the dynamics of the combined system starts with an initial condition on the isochron of the phase that the system is in before the connection. While automatic synchronization methods exist, their performance is not always reliable and most systems use a combination of manual, semi-automatic, and automatic synchronizing schemes [40].

Isochrons of a stable periodic orbit Γ were first introduced by Winfree [43] in 1974. In this paper he provides formal definitions for the notions of *asymptotic phase* (which Winfree calls latent phase) and *isochron* that we reformulate in Definitions 2.1 and 2.2 of the next section. Except for simple examples, isochrons cannot be calculated analytically and one has to resort to numerical approximations. Unfortunately, biological oscillators typically give rise to models with multiple time scales, which are rather sensitive to numerical integration. Therefore, research has been focused on studying the phase-shift of an oscillation due to an infinitesimal, impulsive perturbation [3, 16, 19, 23]. By considering the shift in phase as a function of the phase at which the perturbation is applied, one obtains the infinitesimal *phase response curve* (PRC) for the system [38]. Effectively, the infinitesimal PRC is defined by the linear approximation of the isochrons in a neighborhood of the periodic orbit. Phase models and PRCs are particularly useful for systems of weakly coupled oscillators [2, 33, 41, 44] and oscillators subject to a stimulus [3, 6, 7, 23, 35].

The PRC only gives information related to infinitesimal perturbations. Recently, interest has shifted to studying the effect of larger perturbation, which requires more global knowledge of the isochrons so that their linear approximation alone is not sufficient. We specifically mention Guckenheimer and Sherwood, whose work is, as yet, only published as a PhD thesis [39], and Guillamon and Huguet, whose paper appeared very recently [22]. Guckenheimer and Sherwood use backward integration methods to approximate the isochrons. Guillamon and Huguet introduce the notion of a phase response surface, based on the computation of isochrons via Fourier expansions; as in [39], the global isochrons are obtained by extending the local approximation via backward integration techniques. Unfortunately, the use of backward integration can be very sensitive, particularly for systems with multiple time scales, and it can be very hard, if not impossible, to compute arbitrarily large extensions of a local isochron. In this paper we present a different method for computing global isochrons that is based on the continuation of a suitably posed two-point boundary value problem; we refer to [10] for an introduction on the continuation of boundary value problems. Our approach is particularly well suited for systems with multiple time scales.

We illustrate our continuation method with the example of a two-dimensional reduced Hodgkin-Huxley model that was considered in [28, 34]. The one-dimensional isochrons of this planar model, which are associated with a unique globally attracting periodic orbit Γ, foliate the phase space in a remarkably complicated way. Winfree poses a number of conjectures in [43] and, in particular, wonders about the geometry of isochrons at the boundary $\partial\mathcal{B}$ of the basin of attraction of Γ. He argues that, under suitable genericity conditions, each isochron must come arbitrarily close to any point on $\partial\mathcal{B}$, which he calls the *phaseless set* [43, Conjecture C in the Appendix]. With the use of our method, we can compute each isochron and show up to unprecedented detail its interaction with an equilibrium that is the only point not contained in the basin of Γ. An important advantage of our method is the fact that we compute each isochron via continuation, which automatically provides an arclength parameterization of it that organizes phase space according to the notion of arclength distance to the periodic orbit. As a result, we are able to visualize Winfree's conjecture for this example. Moreover, we find a bounded set of points in the *interior* of the basin of Γ with properties that are very similar to those of a phaseless set.

This paper is organized as follows. In the next section we give formal definitions and present a background of the computational methods for obtaining linear approximations of the isochrons. Section 3 describes how we compute isochrons via continuation of a two-point boundary value problem. The computations can be done, for example, using the software package AUTO [11], and we give specific details on how to formulate the two-point boundary value problem for this purpose. Section 4 discusses in detail the geometry of isochrons computed for a reduced Hodgkin-Huxley model. We end with a discussion in section 5.

2. Definitions and background. Let us begin with a precise definition of an isochron. Consider an autonomous vector field

$$\frac{d\mathbf{x}}{dt} = F(\mathbf{x}), \tag{2.1}$$

with solutions $\mathbf{x} = \mathbf{x}(t)$ that satisfy $\mathbf{x}(0) = \mathbf{x}_0 \in \mathbb{R}^n$; here, $\mathbb{R}^n$ is the phase space of (2.1). In this paper we consider planar vector fields, that is, $n = 2$, so that the isochrons are one dimensional. In principle, it is not essential to have $n = 2$ in what follows and we come back to this in section 5. We assume that F is sufficiently smooth, that is, F is at least C^1. The vector field (2.1) induces a flow $\Phi : \mathbb{R} \times \mathbb{R}^n \to \mathbb{R}^n$ and we will use the notations $\Phi(t, \mathbf{x}_0) = \Phi^t(\mathbf{x}_0)$. We further assume that (2.1) has a orbit Γ with period T_Γ and Γ is a hyperbolic attractor, that is, all Floquet multipliers of Γ lie inside the complex unit circle, except for the trivial multiplier 1 associated with the direction tangent to Γ. We associate a phase with points on Γ as follows. Let $\gamma_0 \in \Gamma$ be the point where the phase is zero; γ_0 is typically chosen as the global maximum of Γ with respect to the first coordinate. Then $\Gamma = \{\Phi(t, \gamma_0) \mid 0 \le t < T_\Gamma\}$ and a point $\gamma_t = \Phi(t, \gamma_0)$ has phase $\theta(\gamma_t) = t/T_\Gamma$. The phase $\theta(\gamma_t)$ takes values in $[0, 1)$, which follows the definition by Winfree [43], but other conventions, such as $[0, 2\pi)$ or $[0, T_\Gamma)$, can easily be obtained via rescaling.

Isochrons are closely related to an extended notion of phase that is also defined for points that do not lie on Γ:

Definition 2.1 (Asymptotic phase). *Let $\mathbf{x}_0 \in \mathbb{R}^n$ be an initial condition for (2.1) that lies inside the basin of attraction of Γ. Then the unique asymptotic phase $\theta(\mathbf{x}_0)$ of $\mathbf{x}_0$ is given by the condition*

$$\lim_{t\to\infty} \| \Phi(t, \mathbf{x}_0) - \Phi(t + \theta(\mathbf{x}_0)\, T_\Gamma, \gamma_0) \| = 0.$$

Hence, the orbit through $\mathbf{x}_0$ *converges asymptotically to* Γ *in the precise sense that it will be in phase with the point* $\Phi(\theta(\mathbf{x}_0)\, T_\Gamma, \gamma_0)$ *on* Γ.

The asymptotic phase is only defined for points $\mathbf{x}_0 \in \mathbb{R}^n$ that lie in the basin $\mathcal{B}(\Gamma)$ of Γ. If Γ is a global attractor of a planar vector field, then $\mathcal{B}(\Gamma)$ is the entire phase space, with the possible exception of one or more unstable equilibria. The complement of $\mathcal{B}(\Gamma)$ is also called the *phaseless set* of Γ.

DEFINITION 2.2 (Isochron). *An isochron is a level set of the asymptotic phase function* $\theta : \mathcal{B}(\Gamma) \subset \mathbb{R}^n \to [0, 1)$*, that is, the collection of all points in the basin of attraction of* Γ *with the same asymptotic phase. We tend to associate isochrons with their corresponding phase points on* Γ*. More precisely, for* $\gamma \in \Gamma$*,*

$$\mathcal{I}(\gamma) = \{\mathbf{x}_0 \in \mathcal{B}(\Gamma) \mid \theta(\mathbf{x}_0) = \theta(\gamma)\}.$$

Since $\mathcal{I}(\gamma)$ is a level set of the asymptotic phase θ, we know that the gradient $\nabla\theta(\gamma)$ evaluated at the base point γ is perpendicular to the tangent of $\mathcal{I}(\gamma)$ at γ; this gradient is typically referred to as the phase response curve [38]. Definition 2.1 implies that isochrons map to each other under the flow, that is, with a slight abuse of notation:

$$\mathcal{I}(\Phi^t(\gamma_0)) = \Phi^t(\mathcal{I}(\gamma_0)).$$

In particular, each isochron $\mathcal{I}(\gamma)$ is invariant under the time-T_Γ map $\Phi^{T_\Gamma}(\cdot)$, which has γ as its fixed point.

We want to consider isochrons from a dynamical systems point of view. Around the same time when Winfree developed his idea of isochrons, Hirsch, Pugh and Shub developed the theory of compact normally hyperbolic invariant manifolds, which culminated in the publication of their book [24] in 1977. For example, Winfree claims in [43, Conjecture A] that isochrons are smooth $(n-1)$-dimensional submanifolds that foliate the basin of attraction of Γ. Quoting from [43]:

> "M. Hirsch assures me that this is proveable (pers. comm.), my "isochrons" being known to topologists as the "stable manifolds" of points on [Γ]."

The paper by Winfree [43] was followed by a publication of Guckenheimer [21] in 1975 that fully explained the questions posed by Winfree [43]. In terms of dynamical systems theory, we may think of Γ as a normally hyperbolic manifold, because we assume that only its trivial Floquet multiplier lies on the complex unit circle. Then the tangent bundle of $\mathbb{R}^n$ over Γ can be split into a linear bundle tangent to Γ and a linear stable normal bundle transverse to Γ that is invariant under the linearization of the flow. Moreover, we can define vector directions associated with these two tangent bundles in the tangent space of $\mathbb{R}^n$ at γ for each point $\gamma \in \Gamma$. Since Γ is a periodic orbit, it is easy to find these vector directions: γ is a fixed point of the time-T_Γ map $\Phi^{T_\Gamma}(\cdot)$ and the tangent and normal vector directions are the eigenvectors of the Jacobian matrix $D\Phi^{T_\Gamma}(\gamma)$ associated with the trivial and nontrivial Floquet multipliers, respectively. The local theory of normally hyperbolic, invariant, compact manifolds [24, §4, Theorem 4.1] ensures the existence of an n-dimensional stable manifold $W^s(\Gamma) = \mathcal{B}(\Gamma)$ that is invariantly fibered (foliated) by $(n-1)$-dimensional submanifolds $W^{ss}(\gamma)$, $\gamma \in \Gamma$ that are as smooth as the function F that defines (2.1). Moreover, $W^s(\Gamma)$ is tangent to the linear stable normal bundle of Γ and each $W^{ss}(\gamma)$ is tangent to the corresponding linear stable eigenspace at γ. By definition, $\mathcal{I}(\gamma) = W^{ss}(\gamma)$, $\gamma \in \Gamma$; see [21, 24, 43].

The interpretation of $\mathcal{I}(\gamma)$ as a leaf $W^{ss}(\gamma)$ of the invariant fibration of $W^s(\Gamma)$ offers a natural way of computing isochrons as stable manifolds, which is precisely

the approach that we take in this paper. Our method is based on the idea of computing stable manifolds via the continuation of orbit segments [15, 30], which assumes knowledge of the periodic orbit Γ as well as the linear approximation of the stable manifold. Before explaining our method, we summarize in the next section several methods for obtaining a *local* approximation of the isochrons.

2.1. Linear approximations of isochrons. The development of computational methods for isochrons has mainly focused on their linear approximations [17, 18, 44]. Indeed, the linear approximation suffices for computing the phase response curve. To our knowledge Guillamon and Huguet [22] are the first to use higher-order approximation methods for the local approximation of isochrons. We briefly discuss these methods here, but primarily focus on the approach that we take for the computations in this paper.

The so-called direct method is based on the formal definition for $\nabla\theta(\gamma)$ as the limit

$$\frac{\partial\theta}{\partial x_i}(\gamma) = \lim_{\Delta x_i \to 0} \frac{\theta(\gamma + \Delta x_i\, \vec{e}_i) - \theta(\gamma)}{\Delta x_i},$$

where $\mathbf{x} = (x_1, x_2, \cdots, x_n)$ and $\vec{e}_i$ denotes the ith basis vector of $\mathbb{R}^n$. The partial derivatives $\frac{\partial}{\partial x_i}\theta(\gamma)$, $i = 1, 2, \ldots, n$ are found by comparing the phase of a base point $\gamma \in \Gamma$ with the phases of solutions in the infinite-time limit starting from points that are infinitesimally shifted from γ [3, 18, 44]. The direct method is a straightforward method that mimics how phase differences are measured in experiments.

The so-called adjoint method views $\nabla\theta(\gamma)$ as an eigenvector for the adjoint of the Jacobian matrix of the time-T_Γ map evaluated at γ. The classical derivation uses Taylor expansions of the orbit through an infinitesimal perturbation of γ; see [3, 16, 26, 17, 27] for more details. However, this approach is essentially the same as computing the linear stable normal bundle of Γ, which defines the linear approximation of $\mathcal{I}(\gamma)$, $\gamma \in \Gamma$. Let us explain this briefly because it is directly related to the method we use in this paper.

Consider the $n \times n$ Jacobian matrix of the time-T_Γ map $\Phi^{T_\Gamma}(\cdot)$ evaluated at γ. Since we assume that Γ is hyperbolic, this matrix $D\Phi^{T_\Gamma}(\gamma)$ has exactly one eigenvalue equal to 1 — the associated eigenvector is the direction tangent to Γ at γ — and the other $n-1$ eigenvalues (counted with multiplicity) are all inside the complex unit circle, that is, they all have modulus less than 1. The $(n-1)$-dimensional hyperplane spanned by the (generalized) eigenvectors associated with these eigenvalues with modulus less than 1 is the linear approximation of $\mathcal{I}(\gamma)$. If $n = 2$ then the linear approximation of $\mathcal{I}(\gamma)$ is simply given by the eigenvector associated with the only stable eigenvalue of $D\Phi^{T_\Gamma}(\gamma)$. As soon as $n > 2$, however, it is more natural to define this linear approximation by a vector perpendicular to $\mathcal{I}(\gamma)$ at γ. Indeed, this perpendicular vector is precisely $\nabla\theta(\gamma)$, and it is given by the left eigenvector $\vec{\mathbf{v}}_\gamma$ associated with the trivial eigenvalue 1 of $D\Phi^{T_\Gamma}(\gamma)$. (Recall that a left eigenvector of a matrix is a right eigenvector of its adjoint.)

The standard method for finding $\vec{\mathbf{v}}_\gamma$ for any base point $\gamma \in \Gamma$ is the power method; the eigenvalue 1 is the largest eigenvalue of (the adjoint of) $D\Phi^{T_\Gamma}(\gamma)$, so an arbitrary vector direction converges to $\vec{\mathbf{v}}_\gamma$ when multiplied iteratively with this matrix. The Jacobian matrix $D\Phi^{T_\Gamma}(\gamma)$ is approximated using finite differencing and the standard method uses backward integration along the periodic orbit Γ. For example, XPP [16] uses this method for finding phase response curves numerically, and Matlab code for this approach can be found in [27, Chapter 10].

2.2. Linear approximation as a two-point boundary value problem. We want to advocate a more direct method for computing $\vec{\mathbf{v}}_\gamma$ and the associated family for all $\gamma \in \Gamma$ that defines the linear stable normal bundle. The idea is to compute Γ and this associated vector bundle in a single two-point boundary value problem; see [12, 13, 32] and, in particular, [9, 19], where this idea is used in the particular context of computing PRCs. Hence, we do not already assume knowledge of Γ. Instead, we combine (2.1) with the first variational equation

$$\left\{ \begin{array}{rcl} \dfrac{d\mathbf{x}}{dt} & = & F(\mathbf{x}), \\ \dfrac{d\vec{\mathbf{v}}}{dt} & = & \mathrm{adj}[DF(\mathbf{x})]\,\vec{\mathbf{v}}. \end{array} \right. \tag{2.2}$$

Here, $\mathrm{adj}[DF(\mathbf{x})]$ is the transpose (or adjoint) of the Jacobian matrix DF of the flow evaluated at a point $\mathbf{x}$ that varies in time according to the first equation of (2.2). Of course, this first equation should define the periodic orbit Γ, so we impose the boundary condition

$$\mathbf{x}(T_\Gamma) = \mathbf{x}(0) =: \gamma, \tag{2.3}$$

where the period T_Γ of Γ is unknown. The first variational equation is the second equation of (2.2). It is linear, but with a time-varying matrix, and its solution is a vector bundle $\vec{\mathbf{v}} = \vec{\mathbf{v}}(t)$. As initial condition, we require $\vec{\mathbf{v}}(0) = \vec{\mathbf{v}}_\gamma \in \mathbb{R}^n$. Note that (2.3) automatically implies that $DF(\mathbf{x})$ and, thus, its adjoint are also periodic; if the linear bundle is orientable, this period is the (unknown) period T_Γ, and if it is non-orientable, we may set up the computation using period $2T_\Gamma$ both for Γ and its normal bundle. Consequently, the vector bundle $\vec{v}$ that is associated with an eigenvector of $D\Phi^{T_\Gamma}(\gamma)$ is periodic in the sense that the vector direction is mapped to itself after one full period, which we denote T_Γ for both orientable and non-orientable cases from now on. Indeed, the length of $\vec{\mathbf{v}}_\gamma$ may shrink or expand by a factor that is equal to the Floquet multiplier associated with this vector bundle. However, we are interested in the vector bundle associated with the trivial Floquet multiplier, so we have

$$\vec{\mathbf{v}}(T_\Gamma) = \vec{\mathbf{v}}(0) =: \vec{\mathbf{v}}_\gamma, \tag{2.4}$$

and we assume that $\vec{\mathbf{v}}_\gamma$ is normalized to 1. The combined system (2.2)–(2.4) is well posed and defines the solution up to a phase condition that fixes γ. Note that the trivial bundle $\vec{\mathbf{v}} \equiv 0$ for Γ is a solution that coexists with the actual eigenvector bundle we are after. Since the trivial bundle is a solution for any Floquet multiplier, one can find the nontrivial vector bundle as a branching solution from the trivial family that bifurcates at the particular Floquet multiplier 1; we refer to [12, 13, 32] for details.

We note here that for planar systems the vector bundle is always orientable. Furthermore, it is just as easy to compute the linear stable normal bundle $\vec{\mathbf{n}}^s$ directly by using

$$\left\{ \begin{array}{rcl} \dfrac{d\vec{\mathbf{n}}^s}{dt} & = & DF(\mathbf{x})\,\vec{\mathbf{n}}^s, \\ \vec{\mathbf{n}}^s(T_\Gamma) & = & \mu^{T_\Gamma}\,\vec{\mathbf{n}}^s(0), \end{array} \right. \tag{2.5}$$

combined with (2.1) and (2.3). Here, μ is the stable Floquet multiplier of Γ. (Note that we use the Jacobian rather than its adjoint here.) Since μ can be extremely close

to 0 in systems with multiple time scales, it can be advantageous to use a logarithmic formulation in terms of the Floquet exponent: By setting $\mu = e^{\lambda}$ and $\vec{\mathbf{n}}^s = e^{\lambda t}\,\vec{\mathbf{w}}$, the equation for the first variational part becomes

$$\begin{cases} \dfrac{d\vec{\mathbf{w}}}{dt} &= DF(\mathbf{x})\,\vec{\mathbf{w}} - \lambda\,\vec{\mathbf{w}}, \\ \vec{\mathbf{w}}(T_\Gamma) &= \vec{\mathbf{w}}(0). \end{cases}$$

We again refer to [12, 13, 32] for details.

2.3. Higher-order local approximations of isochrons. We end with a brief discussion of higher-order methods. As mentioned, the first such method in the context of computing local approximations of isochrons was published only recently in [22]. However, any higher-order method for computing local stable manifolds can be adapted for this purpose. Guillamon and Huguet [22] use the so-called parameterization method that is originally designed for computing invariant manifolds [4], that is, they view the isochron $\mathcal{I}(\gamma)$ as a leaf of the invariant fibration of the stable manifold of Γ at γ. The parameterization method uses Fourier expansions to represent the manifold. It appears that Fourier expansions are not ideal for systems with multiple time scales, because the convergence of the expansion is typically slow and many terms are needed; see [22] for details. It should be expected that any higher-order approximation method will be applicable only in a (possibly large) neighborhood of Γ. Also in [22] the parameterization method is only used for computing a local approximation of $\mathcal{I}(\gamma)$, which is then extended by other means to obtain a global approximation of the isochron.

3. Extending the isochrons. Globally, the isochrons are nonlinear (immersed) manifolds formed by the leaves of the invariant fibration of the stable manifold of the periodic orbit Γ [21, 24]. More precisely, the isochron $\mathcal{I}(\gamma)$ of a point $\gamma \in \Gamma$ is the stable manifold $W^{ss}(\gamma)$ that is invariant under the time-T_Γ map $\Phi^{T_\Gamma}(\cdot)$ that has γ as its fixed point. The dynamics on $\mathcal{I}(\gamma)$ generated by $\Phi^{T_\Gamma}(\cdot)$ is a contraction, that is, $\mathcal{I}(\gamma)$ is an overflowing manifold and any local approximation can be extended by inverse iterations of $\Phi^{T_\Gamma}(\cdot)$. The methods described in Sections 2.1–2.3 can be used to obtain a local approximation of $\mathcal{I}(\gamma)$ that is valid only in a small neighborhood of Γ. Throughout this section we focus on planar vector fields, that is, $\mathcal{I}(\gamma)$ is one dimensional. Then we can employ standard techniques for the computation of global stable manifolds to compute global extensions of $\mathcal{I}(\gamma)$; see, for example, the discussion of such methods in [29].

To our knowledge, iterates of the inverse of $\Phi^{T_\Gamma}(\cdot)$ have thus far been computed by numerical integration. The most straightforward way is to integrate the flow backward in time [22, 39]. However, for systems with multiple time scales, backward integration is numerically extremely sensitive. For this reason, forward integration techniques using shooting have also been employed [5]. Both cases view the manifold as a collection of (backward) iterates of a chosen fundamental domain on the local approximation. A fundamental domain is a segment on the local approximation with the property that one end point maps to the other end point, so that subsequent backward iterates form a connected curve. Each extension is generated such that its mesh is distributed uniformly or according to local curvature properties of the manifold. Unfortunately, the dynamics of the system — and this applies in particular to systems with multiple time scales — may depend sensitively on the initial condition. Therefore, it becomes increasingly difficult to generate an accurate mesh on higher

iterates of the fundamental domain, and methods using numerical integration tend to break down after a relatively short number of iterations. In fact, also for single-time-scale systems it can be difficult to generate an ordered sequence of points that effectively parameterizes the isochron by arclength.

In the next section we propose a new method for computing global extensions of isochrons based on the continuation of a two-point boundary value problem [30]. The accuracy of the method does not depend solely on the initial condition, but uses information of the flow along entire orbit segments. Furthermore, the continuation automatically generates a mesh parameterized by arclength.

3.1. Global isochrons as a family of orbit segments. The method we propose for computing global extensions of isochrons is also based on the idea of viewing the isochron $\mathcal{I}(\gamma)$ of a point $\gamma \in \Gamma$ as a stable manifold $W^{ss}(\gamma)$ of $\Phi^{T_\Gamma}(\cdot)$. The set-up is very similar to that in [15] for the computation of one-dimensional manifolds of the fixed point of a Poincaré map that is associated with a periodic orbit of the underlying vector field. Indeed, the isochron of a point γ on Γ is nothing but the Poincaré section through γ of the time-T_Γ return map $\Phi^{T_\Gamma}(\cdot)$. In [15] the Poincaré section is known and the associated Poincaré map is unknown, but defined implicitly as the (local) return to this section. In the present setting, the Poincaré map is defined as the time-T_Γ map and the associated section is not known. If (2.1) were a periodically forced system with forcing period T_Γ, then the Poincaré section of the time-T_Γ map would be the phase space at fixed T_Γ-periodic time intervals. Hence, for this special case both the Poincaré map and the section are known explicitly. In general, however, the section associated with the time-T_Γ map is defined implicitly by the fact that points return to it after precisely the period T_Γ of Γ. This unknown Poincaré section is precisely the isochron $\mathcal{I}(\gamma)$ that we wish to compute.

Just as for the integration methods mentioned above, we assume knowledge of a first local approximation of the isochron $\mathcal{I}(\gamma)$. We find that the linear approximation is sufficient for finding good global approximations of $\mathcal{I}(\gamma)$ [29, 36]. Particularly in the context of systems with multiple time scales, the contraction rates along the manifolds are extremely strong, which means that one can start with a local approximation in a very small neighborhood of Γ and still grow the manifold rapidly away from Γ. We compute the linear approximation of $\mathcal{I}(\gamma)$ with the method described in section 2.2. Let us assume that we have computed the vector direction $\vec{\mathbf{v}}_\gamma \in \mathbb{R}^2$ that is perpendicular to the linear approximation $\vec{\mathbf{n}}^s_\gamma \in \mathbb{R}^2$ of $\mathcal{I}(\gamma)$. We define the line segment

$$L_\eta(\gamma) := \{\gamma + \delta \vec{\mathbf{n}}^s_\gamma \mid 0 \leq |\,\delta\,| \leq \eta\}, \tag{3.1}$$

parameterized by δ. For $\eta \ll 1$ this line segment gives a good approximation of $\mathcal{I}(\gamma)$, and we denote points on it by $L_\eta(\gamma;\delta)$.

We view $\mathcal{I}(\gamma)$ as defined by a one-parameter solution family of a two-point boundary value problem (BVP). In the notation of AUTO [11] this BVP is formulated as follows. We consider orbit segments $\{\mathbf{u}(t) \mid 0 \leq t \leq 1\}$ that correspond to orbit segments $\{\mathbf{x}(t) \mid 0 \leq t \leq T_\Gamma\}$ of (2.1). That is, we consider orbit segments of the rescaled vector field

$$\dot{\mathbf{u}} = T_\Gamma\, F(\mathbf{u}). \tag{3.2}$$

An orbit segment corresponds to a point on $\mathcal{I}(\gamma)$ if both $\mathbf{u}(0)$ and $\mathbf{u}(1)$ are on $\mathcal{I}(\gamma)$. Note that the two points $\mathbf{u}(0)$ and $\mathbf{u}(1)$ are related, because we keep T_Γ fixed. The

idea is now to find $\mathbf{u}(0)$ such that $\mathbf{u}(1)$ lies on the *numerical approximation* of $\mathcal{I}(\gamma)$. Initially, all we have is the linear approximation of $\mathcal{I}(\gamma)$, which leads to the boundary condition

$$\mathbf{u}(1) = L_\eta(\gamma; \delta). \tag{3.3}$$

for some δ with $0 \leq |\,\delta\,| \leq \eta \ll 1$, where η is prespecified. The fact that we keep T_Γ fixed serves as a second condition, giving a unique solution for given δ. We can now solve the BVP (3.2)–(3.3) by continuation, where we keep T_Γ fixed and use δ as a free parameter. The periodic orbit Γ starting at γ solves (3.2)–(3.3) for $\delta = 0$. Hence, the continuation can be started from the known solution

$$\mathbf{u}_{\text{start}} := \{\mathbf{u}(t) \mid 0 \leq t \leq 1,\ \mathbf{u}(0) = \mathbf{u}(1) = \gamma\}. \tag{3.4}$$

We use AUTO [11] for the continuation and let δ vary from 0 to η. Since AUTO [11] adapts the continuation step size automatically, we obtain a good distribution of points along the isochron and can easily monitor the arclength of the approximation. The major advantage of this method over the integration methods mentioned earlier is the fact that AUTO [11] measures the variation between two orbit segments along the entire orbit segment and not just at the initial value. This avoids the extreme sensitivity on initial conditions that is so typical for multiple-time-scale systems. As a result, we are able to compute isochrons up to unprecedented arclengths.

The continuation of the BVP (3.2)–(3.3) extends the isochron $\mathcal{I}(\gamma)$ from the linear approximation $L_\eta(\gamma)$ of arclength $2\eta \ll 1$ up to a longer nonlinear approximation that typically has an arclength of order $O(1)$ for multiple-time-scale systems. There are two different techniques to extend $\mathcal{I}(\gamma)$ further. In the spirit of [15], one can change the boundary condition (3.3) to restrict $\mathbf{u}(1)$ to the new longer approximation of $\mathcal{I}(\gamma)$. This works well as long as the curvature along $\mathcal{I}(\gamma)$ does not grow very large. For the example in section 4 we use a different technique: we perform continuation for the time-$(2T_\Gamma)$ map, that is, we compute the family of orbit segments that return to $L_\eta(\gamma)$ after two full periods T_Γ of Γ, then for the time-$(3T_\Gamma)$ map, and so on, as follows. Suppose that after the continuation for the time-$((k-1)T_\Gamma)$ map, we have $\delta = \eta$ and the corresponding solution is

$$\begin{aligned}\mathbf{u}^\star &:= \{\mathbf{u}(t) \mid 0 \leq t \leq 1,\ \mathbf{u}(1) = L_\eta^\gamma(\eta)\} \\ &= \{\mathbf{x}(t) \mid 0 \leq t \leq (k-1)\,T_\Gamma,\ \mathbf{x}((k-1)\,T_\Gamma) = L_\eta(\gamma;\eta)\}.\end{aligned}$$

We then start a new continuation run, where we solve

$$\dot{\mathbf{u}} = kT_\Gamma\, F(\mathbf{u}),$$

with the same boundary condition (3.3) as before. The continuation can be started by concatenating the solutions $\mathbf{u}^\star$ and $\mathbf{u}_{\text{start}}$ and rescaling them back to the $[0,1]$ interval. That is, we define

$$\mathbf{u}(t) = \begin{cases} \mathbf{u}(t) = \mathbf{u}^\star(k\,t), & 0 \leq t \leq \frac{k-1}{k}, \\ \mathbf{u}(t) = \mathbf{u}_{\text{start}}(k\,(t-1)+1), & \frac{k-1}{k} < t \leq 1. \end{cases} \tag{3.5}$$

Of course, the concatenation contains a small discontinuity (or jump) at $t = \frac{k-1}{k}$, but as a seed solution for Newton's method, this will typically converge to a proper solution and successfully start the continuation. If the convergence fails because the

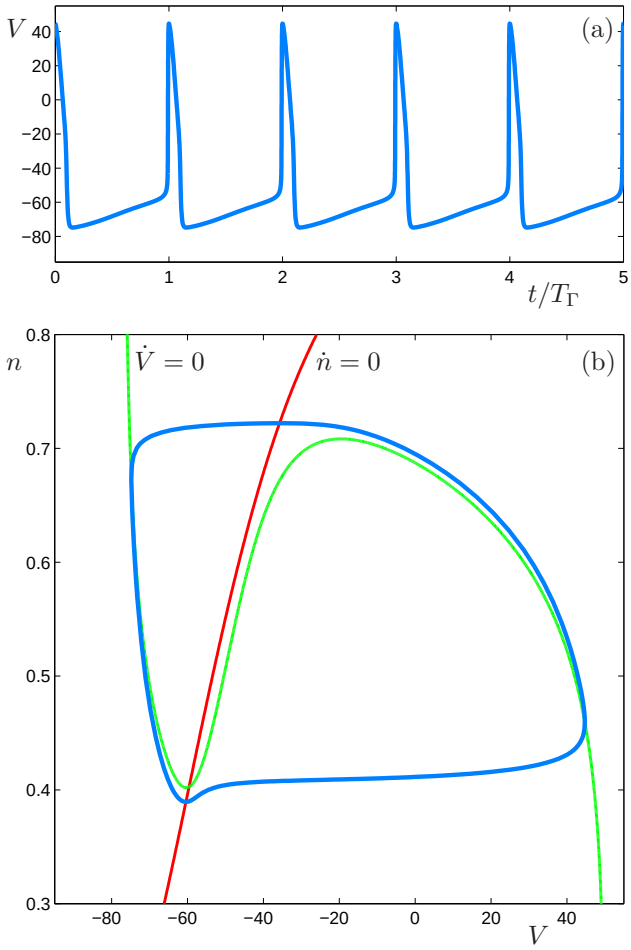

FIG. 1. *The stable periodic orbit* Γ *(blue) of the reduced Hodgkin-Huxley model* (4.1). *Panel (a) shows the time series of the* V*-coordinate of* Γ*, which emphasizes the slow-fast nature of the model; panel (b) shows* Γ *in phase space along with the* V*-nullcline (green) and the* n*-nullcline (red) that intersect at the source.*

discontinuity is too large, then more advanced techniques based on Lin's method can be employed; see [32] and references therein for details.

We used the new Python interface for AUTO [11] to implement our method such that it automatically computes an arbitrary number of isochrons uniformly distributed in time or arclength along the periodic orbit up to any prespecified number of returns. We illustrate the performance of our method with the example in the next section.

4. Isochrons of the reduced Hodgkin-Huxley model. To illustrate the method for computing isochrons, we consider a two-dimensional reduced model of the Hodgkin-Huxley equations [25]. The model is based on the dynamical interplay between ionic conductances and electrical activity using the voltage V, and three gating variables, denoted m, n, and h, for the conductance channels. In the reduced planar model the gating variable m is replaced by its quasi-steady-state function $m_\infty(V)$, and the gating variable h is replaced by $0.8-n$, which is a good approximation of its average value; see [27, 28, 34]. The reduced model of the Hodgkin-Huxley can

then be written as the vector field

$$\begin{cases} \dot{V} &= \frac{1}{C}\left[I_{\text{app}} - \bar{g}_{Na}\,[m_\infty(V)]^3\,(0.8-n)\,(V-V_{Na})\right. \\ & \quad \left. -\bar{g}_K\,n^4\,(V-V_K) - g_L(V-V_L)\right], \\ \dot{n} &= \alpha_n(V)\,(1-n) - \beta_n(V)\,n, \end{cases} \tag{4.1}$$

where

$$\begin{aligned} \alpha_n(V) &= \frac{0.01(V+55)}{1-\exp[-(V+55)/10]}, & \beta_n(V) &= 0.125\exp\left(\frac{-(V+65)}{80}\right), \\ \alpha_m(V) &= \frac{0.1(V+40)}{1-\exp[-(V+40)/10]}, & \beta_m(V) &= 4\exp\left(\frac{-(V+65)}{18}\right), \\ m_\infty(V) &= \frac{\alpha_m(V)}{\alpha_m(V)+\beta_m(V)}, \end{aligned}$$

and the parameters are given by

$$\begin{array}{rclrclrcl} \bar{g}_{Na} &=& 120, & \bar{g}_K &=& 36, & g_L &=& 0.3, \quad I_{\text{app}} = 10, \\ V_{Na} &=& 50, & V_K &=& -77, & V_L &=& -54.4, \quad C = 1. \end{array}$$

System (4.1) has a stable periodic orbit Γ with period $T_\Gamma \approx 11.8463$; it is shown in Figure 1. Panel (a) gives the time series of Γ for the V-coordinate. The time series illustrates that Γ is a relaxation oscillation organized by the much slower dynamics of n relative to the dynamics of V. Panel (b) shows Γ in (V,n)-space along with the nullclines $\dot{V}=0$ and $\dot{n}=0$ in green and red, respectively. The nullclines intersect approximately at $\mathbf{x}^* := (V,n) \approx (-59.6044, 0.4026)$, which is the only equilibrium of (4.1). This equilibrium is a source with complex eigenvalues.

The slow-fast nature of (4.1) also has an effect on the location of the isochrons. Figure 2 shows the isochrons of one hundred points $\gamma_i = \Phi^{\theta_i T_\Gamma}(\gamma_0) \in \Gamma$ with phases $\theta_i = \frac{i}{100}$, for $i = 0, 1, \ldots, 99$. Here, we associate zero phase with the point $\gamma_0 := (V,n) \approx (44.7064, 0.4597)$ on Γ where V is maximal; note that γ_0 must then lie on the V-nullcline. As can be seen in Figure 2, most isochrons start at points on Γ that are located close to the left branch of the V-nullcline (Γ intersects the left branch of the V-nullcline at only one point); this means that the phase changes most rapidly with respect to arclength along this segment of Γ.

Each isochron in Figure 2 has two branches, one on the outside of Γ and one on the inside. The branches on the outside of Γ go off to infinity with asymptotes that are almost horizontal. Indeed, the dynamics of points outside and far away from Γ is dominated by the V-velocity and their asymptotic phase is mostly determined by their n-coordinates. Since the isochrons foliate the entire basin of Γ, which is the plane except for the equilibrium $\mathbf{x}^*$, the branches of the isochrons inside Γ must end up at $\mathbf{x}^*$, which is the phaseless set of (4.1). However, Figure 2 seems to show isochrons that bend away from $\mathbf{x}^*$ and the accumulation onto $\mathbf{x}^*$ is not at all obvious. In the next section we focus on the specific behavior of a single isochron to investigate this seeming contradiction.

4.1. The 0-phase isochron. The isochron branches inside Γ do end up at the equilibrium $\mathbf{x}^*$, but the accumulation process is rather complicated. Figure 3 shows the 0-phase isochron of Γ, that is, for the point γ_0 with maximal V that lies on the intersection of Γ with the V-nullcline. The linear approximation of the isochron is

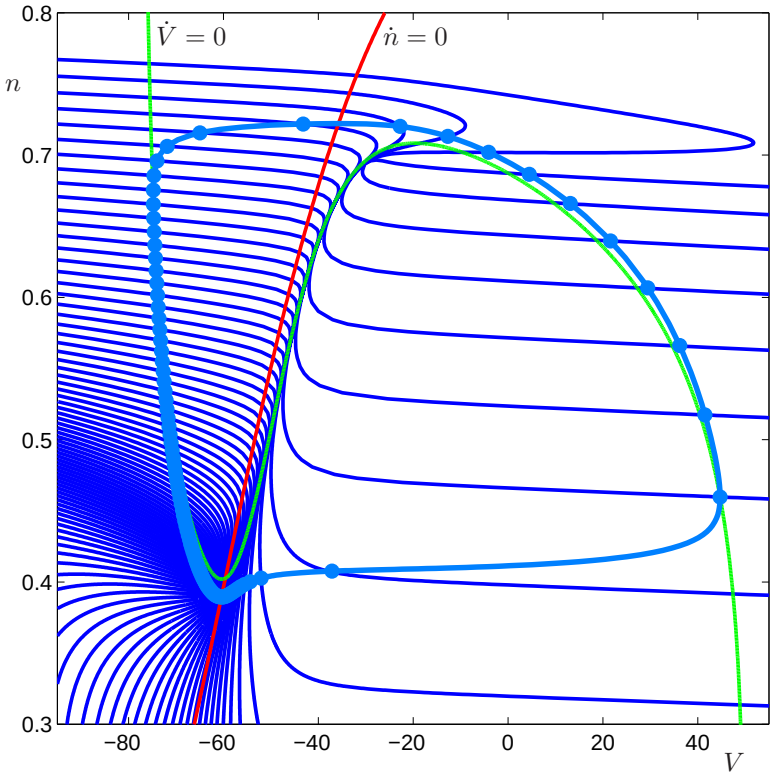

FIG. 2. *A total of 100 isochrons (dark blue) uniformly distributed in time along the stable periodic orbit (blue) of the reduced Hodgkin-Huxley model* (4.1). *The V-nullcline (green) and the n-nullcline (red) are included for reference.*

almost horizontal here and we found $\vec{v}_{\gamma_0} := (0.99999988, -0.00013711)$. Figure 3(a) shows the isochron $\mathcal{I}(\gamma_0)$ computed up to the time-$(4T_\Gamma)$ map for a maximum distance of $\delta = \eta = 10^{-4}$ on the linear approximation. By moving a point along $\mathcal{I}(\gamma_0)$ starting at γ_0, we illustrate with the accompanying animation `anim-hhiso00.gif` how the inside branch approaches $\mathbf{x}^*$. The equilibrium $\mathbf{x}^*$ is not labeled in the figure, but it lies at the intersection of the two nullclines. In panel (b), the n-coordinate along $\mathcal{I}(\gamma_0)$ is plotted versus its arclength, where the arclength is 0 at γ_0. We see that $\mathcal{I}(\gamma_0)$ initially stays almost horizontal (it is roughly linear) until it comes close to the V-nullcline. Then, instead of approaching $\mathbf{x}^*$ directly, $\mathcal{I}(\gamma_0)$ bends around and moves away from $\mathbf{x}^*$ while it closely follows the V-nullcline. At some maximum value $n \approx 0.6802$, where the arclength of $\mathcal{I}(\gamma_0)$ is a little over 100, the isochron bends back virtually on top of itself towards $\mathbf{x}^*$. We call this behavior of the isochron an 'excursion.' After this first excursion, $\mathcal{I}(\gamma_0)$ makes a counter-clockwise loop around $\mathbf{x}^*$ before moving back up along the V-nullcline. During this second excursion, $\mathcal{I}(\gamma_0)$ does not come as high as during the first, reaching $n \approx 0.5517$. On the way down $\mathcal{I}(\gamma_0)$ first makes a clockwise loop around $\mathbf{x}^*$ before turning around making a counter-clockwise loop and moving back up for the third excursion. Figure 3(c) shows an enlargement near $\mathbf{x}^*$, where we can see the switches to counter-clockwise loops as relatively sharp turns, which we call 'boomerang turns,' The continuation up to the time-$(4T_\Gamma)$ map gives three excursions and three boomerang turns that form a spiral pattern that converges to $\mathbf{x}^*$. We find

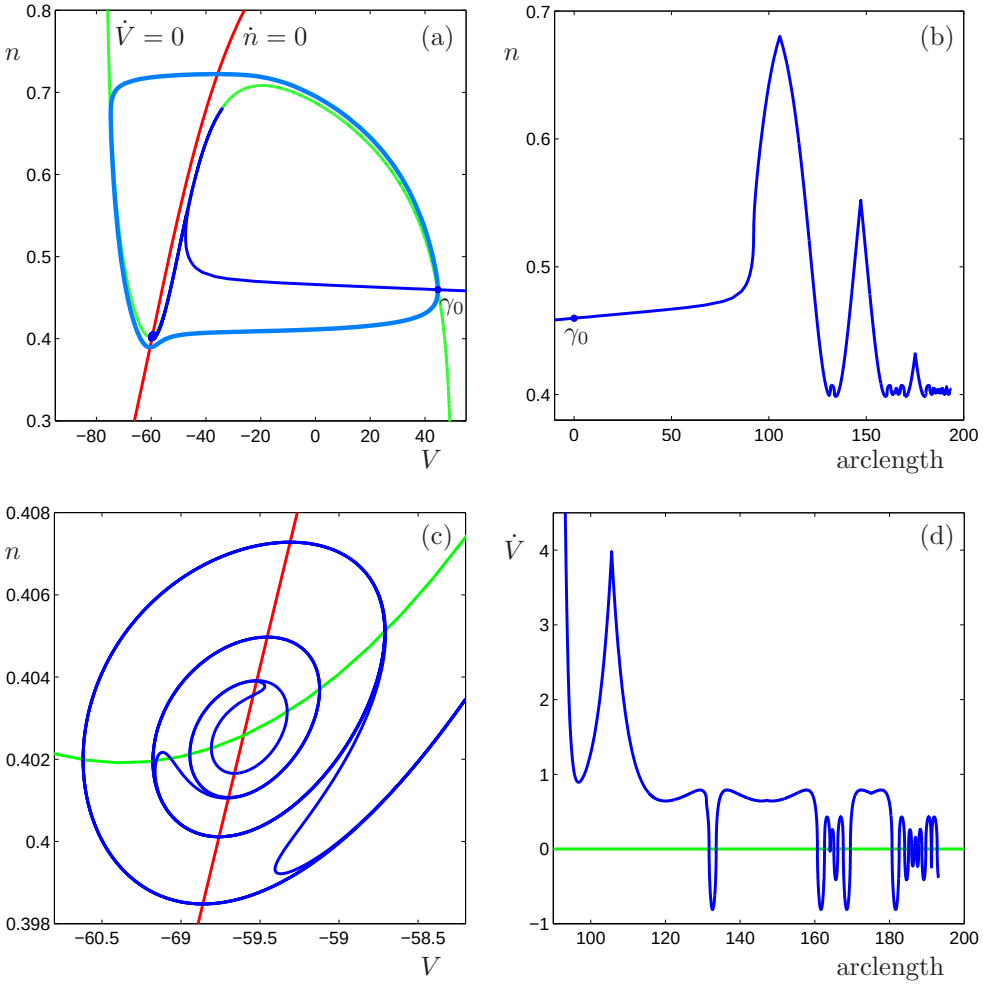

FIG. 3. *The 0-phase isochron $\mathcal{I}(\gamma_0)$ (dark blue) of the point γ_0 on the stable periodic orbit (blue) of the reduced Hodgkin-Huxley model* (4.1). *Panel (a) shows $\mathcal{I}(\gamma_0)$ in the phase plane, where the V-nullcline (green) and the n-nullcline (red) are included for reference; panel (b) shows the n-coordinate of $\mathcal{I}(\gamma_0)$ versus its arclength; panel (c) is an enlargement to illustrate the accumulation onto the equilibrium $\mathbf{x}^*$ (not labeled); panel (d) shows the value of $\dot{V}$ along $\mathcal{I}(\gamma_0)$ versus its arclength, where $\dot{V}>0$ below the V-nullcline (green) in panel (c) and $\dot{V}<0$ above it. The associated animation* `anim-hhiso00.gif` *shows a point moving along the inside branch of $\mathcal{I}(\gamma_0)$.*

more excursions that involve an increasingly larger number of clockwise-loops before a boomerang turn if we perform continuation for the time-(kT_Γ) map with $k>4$. Panel (d) shows the value of $\dot{V}$ versus the arclength of $\mathcal{I}(\gamma_0)$ to illustrate that $\mathcal{I}(\gamma_0)$ does not actually lie on the V-nullcline. In fact, it only intersects the V-nullcline when it loops around $\mathbf{x}^*$; the V-nullcline is the horizontal 0-axis (green) in Figure 3(d).

4.2. Global properties of the 0-phase isochron. The fact that we are able to compute the isochron $\mathcal{I}(\gamma_0)$ to great accuracy as a one-dimensional curve allows us to study its properties in unprecedented detail. The excursions of $\mathcal{I}(\gamma_0)$ create curve segments that are extremely close to each other. By definition, each point on these curve segments arrives under the flow on the linear approximation $L_\eta(\gamma_0)$ with

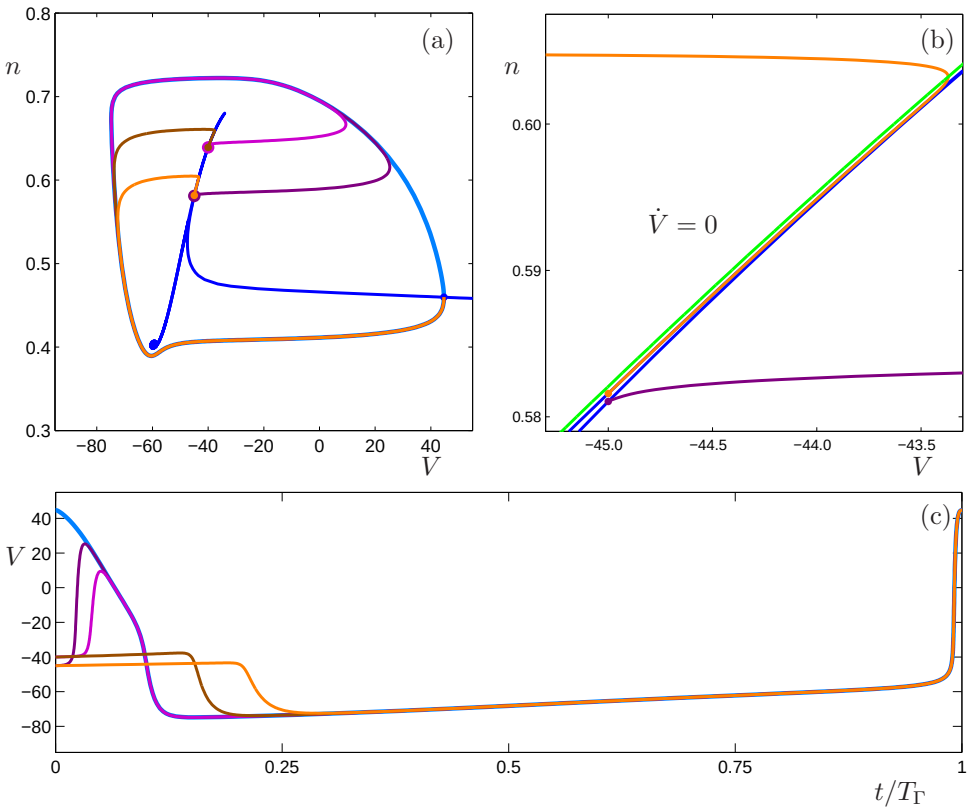

FIG. 4. *Pairs of jump-right and jump-left orbits at* $V = -45.0$ *and* $V = -40.0$ *on the* 0*-phase isochron (dark blue) of the reduced Hodgkin-Huxley model* (4.1). *All four orbit segments lie on* $L_\eta(\gamma_0)$ *with* $\eta = 10^{-4}$ *after one period. Panel (a) shows the phase plane; panel (b) is an enlargement illustrating that a jump-left orbit lies to the right of the* V*-nullcline (green); panel (c) shows the time series of* V *for these four orbit segments over one period, overlaid on the corresponding time series for the periodic orbit (blue). The associated animations* `anim-hhPOiso04.gif` *and* `anim-hhPOiso06.gif` *show the in-phase convergence of a jump-right orbit at* $V = -40.0$ *and a jump-left orbit at* $V = -45.0$*, respectively.*

$\eta = 10^{-4}$ at *exactly the same time* modulo the period T_Γ. Hence, each points identifies a unique orbit segment in the one-parameter family of orbit segments that solves the BVP (3.2)–(3.3). Figure 4 shows four such orbit segments associated with four points along $\mathcal{I}(\gamma_0)$; they form two pairs, one with $V = -45.0$ and one with $V = -40.0$, that lie on corresponding pairs of segments of the first excursion. The phase portrait in panel (a) illustrates that one of the orbit segments in each pair suddenly moves to the left as it converges to Γ, while the other moves to the right; we call them jump-left and jump-right orbits, respectively. This does not necessarily mean that their initial conditions must lie on opposite sides of the V-nullcline, as is illustrated in Figure 4(b) for the pair with $V = -45.0$. Indeed, the jump-left orbit closely follows the V-nullcline and moves to the right until it crosses the V-nullcline before making the jump. Figure 4(c) shows the time series of the orbit segments; here, the jump-right orbits move up and the jump-left orbits move down before converging to Γ. These moves are indeed very fast in time, which is why we refer to them as jumps. The initial plateaus in panel (c), particularly of the jump-left orbits, illustrate how the

orbit segments linger close to the repelling branch of the V-nullcline in order to jump at exactly the right moment to meet $L_\eta(\gamma_0)$ after period T_Γ; see also the animations `anim-hhPOiso04.gif` and `anim-hhPOiso06.gif`.

Figure 4(b) shows that pairs of jump-right and jump-left orbits that start with the same V-coordinate do not straddle the repelling branch of the V-nullcline. However, they must straddle the corresponding repelling slow manifold. A repelling slow manifold S^r_ε consists of all points with forward trajectories that stay $O(\varepsilon)$ close to the repelling branch of the critical manifold for $O(1)$ time, delimited by folds with respect to the fast flow; here, $0 < \varepsilon \ll 1$ represents the (local) ratio between the slow and fast time scales and for the reduced Hodgkin-Huxley model (4.1) the critical manifold is the one-dimensional V-nullcline, with the repelling branch in between its local maximum and minimum. We refer to [1, 14] for more details on slow manifolds and their effects on the dynamics of the system. Since a slow manifold has the same dimension as the corresponding critical manifold, (4.1) has a one-dimensional repelling slow manifold S^r_ε that consist of a single orbit segment very close to the repelling branch of the V-nullcline. Hence, S^r_ε is an orbit segment, and neither jump-left nor jump-right orbits can cross it. The 0-phase isochron $\mathcal{I}(\gamma_0)$ winds around S^r_ε, with jump-left orbits starting from points on $\mathcal{I}(\gamma_0)$ that lie to the left of S^r_ε and jump-right orbits starting from points on $\mathcal{I}(\gamma_0)$ that lie to the right of it. Note that the points that correspond to jump-left orbits must lie closer to S^r_ε than those that correspond to jump-right orbits, because they linger near the V-nullcline for longer.

The second excursion of $\mathcal{I}(\gamma_0)$ consists of two segments that lie even closer to S^r_ε. Points on these segments correspond to orbit segments that reach $L_\eta(\gamma_0)$ after two periods T_Γ. This is illustrated in Figure 5. Panels (a) and (b) show phase portraits of two pairs of jump-right and jump-left orbits at $V = -55.0$ and $V = -50.0$, respectively. These orbits must follow S^r_ε for a relatively longer time, so that they only reach $L_\eta(\gamma_0)$ after the second full period; see their time series shown in panel (c). As in Figure 4(c), the jump-right orbits have the longest plateaus in Figure 5(c) and the jump-left orbits almost reach $L_\eta(\gamma_0)$ already during the first period.

The change from jump-right to jump-left orbits is continuous, by which we mean that the segments on $\mathcal{I}(\gamma_0)$ that correspond to jump-right and jump-left orbits are separated by short segments along which the concept of a left or right jump is not well defined. Indeed, close to the maximum of an excursion $\mathcal{I}(\gamma_0)$ intersects S^r_ε. The repelling slow manifold S^r_ε is really a segment of an orbit $\mathbf{x}^r = \mathbf{x}^r(t)$ that converges to Γ. While it is not clear where $\mathbf{x}^r$ ceases to correspond to S^r_ε, the points on $\mathcal{I}(\gamma_0)$ near its intersection with S^r_ε correspond to orbits that closely follow $\mathbf{x}^r$ and they do not really 'jump.'

As $\mathcal{I}(\gamma_0)$ loops around $\mathbf{x}^*$, there is no nearby repelling slow manifold, although the orbit $\mathbf{x}^r$ that corresponds to S^r_ε continues all the way backward in time to $\mathbf{x}^*$. The points on segments of $\mathcal{I}(\gamma_0)$ near $\mathbf{x}^*$ also correspond to orbit segments that cannot easily be distinguished as jump-right or jump-left orbits. Figure 6 illustrates the behavior of the orbits generated from points on a part of $\mathcal{I}(\gamma_0)$ that loops around $\mathbf{x}^*$. We picked four orbit segments that all start on $\mathcal{I}(\gamma_0)$ with $V = -59.2$ and end on $L_\eta(\gamma_0)$ with $\eta = 10^{-4}$ after two periods T_Γ; the orbit segments are colored purple, magenta, brown, and orange in the order of their initial conditions on $\mathcal{I}(\gamma_0)$. The orbit segments are shown in Figure 6(a), with an enlargement near $\mathbf{x}^*$ in panel (b) and their time series in panel (c). Particularly in Figure 6(c) it is hard to decide whether the orbit segments actually jump. Their initial conditions are shown in Figure 6(b); note that even in this enlargement the first (purple) and last (orange) of these points lie

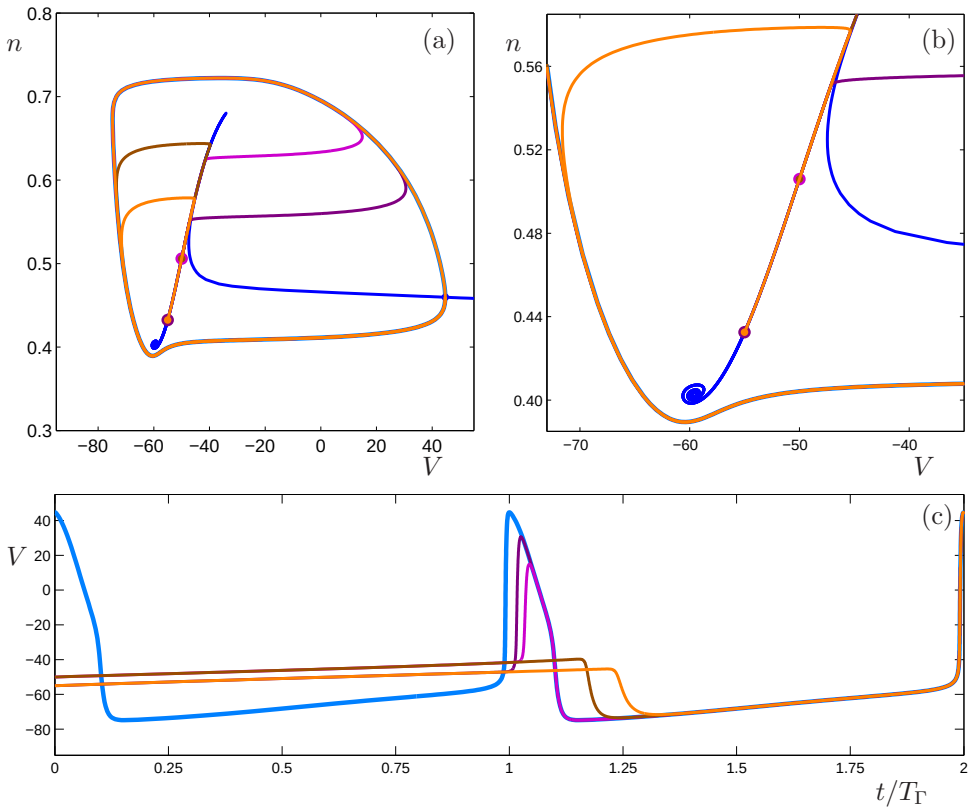

FIG. 5. *Pairs of jump-right and jump-left orbits at* $V = -55.0$ *and* $V = -50.0$ *on the* 0*-phase isochron (dark blue) of the reduced Hodgkin-Huxley model* (4.1). *All four orbit segments lie on* $L_\eta(\gamma_0)$ *with* $\eta = 10^{-4}$ *after two periods. Panel (a) shows the phase plane, with an enlargement in panel (b); panel (c) shows the time series of* V *for these four orbit segments over two periods, overlaid on corresponding time series for the periodic orbit (blue). The associated animations* `anim-hhPOiso16.gif` *and* `anim-hhPOiso18.gif` *show the in-phase convergence of a jump-right orbit at* $V = -55.0$ *and a jump-left orbit at* $V = -50.0$*, respectively.*

virtually on top of each other. Following $\mathcal{I}(\gamma_0)$ down from the top-right (which is covered by orange from the last orbit), the first (purple) orbit starts at the end of the first excursion just before $\mathcal{I}(\gamma_0)$ makes a counter-clockwise loop around $\mathbf{x}^*$; this segment of the first excursion corresponds to jump-left orbits. The purple orbit does turn to the left, but it only makes a small loop around $\mathbf{x}^*$ before moving to the right instead. Similarly, the second (magenta) orbit starts immediately after the first boomerang turn of $\mathcal{I}(\gamma_0)$ and makes a left turn in the sense that it loops around $\mathbf{x}^*$ before moving right. The third (brown) orbit segment starts into the counter-clockwise loop and traces $\mathcal{I}(\gamma_0)$ back for a while before making a right jump; see Figure 6(a). One could say that this (brown) orbit closely follows the orbit $\mathbf{x}^r$ and, in fact, apart from the boomerang turns on $\mathcal{I}(\gamma_0)$, there is a clear spiraling curve that seems to trace $\mathbf{x}^r$. Indeed, part of the last (orange) orbit segment lies almost on top of the brown orbit segment, but its starting point lies only past the loop around $\mathbf{x}^*$. This orbit segment has the distinct features of a jump-right orbit, marking the start of the second excursion.

The second excursion of $\mathcal{I}(\gamma_0)$ must necessarily intersect the repelling slow man-

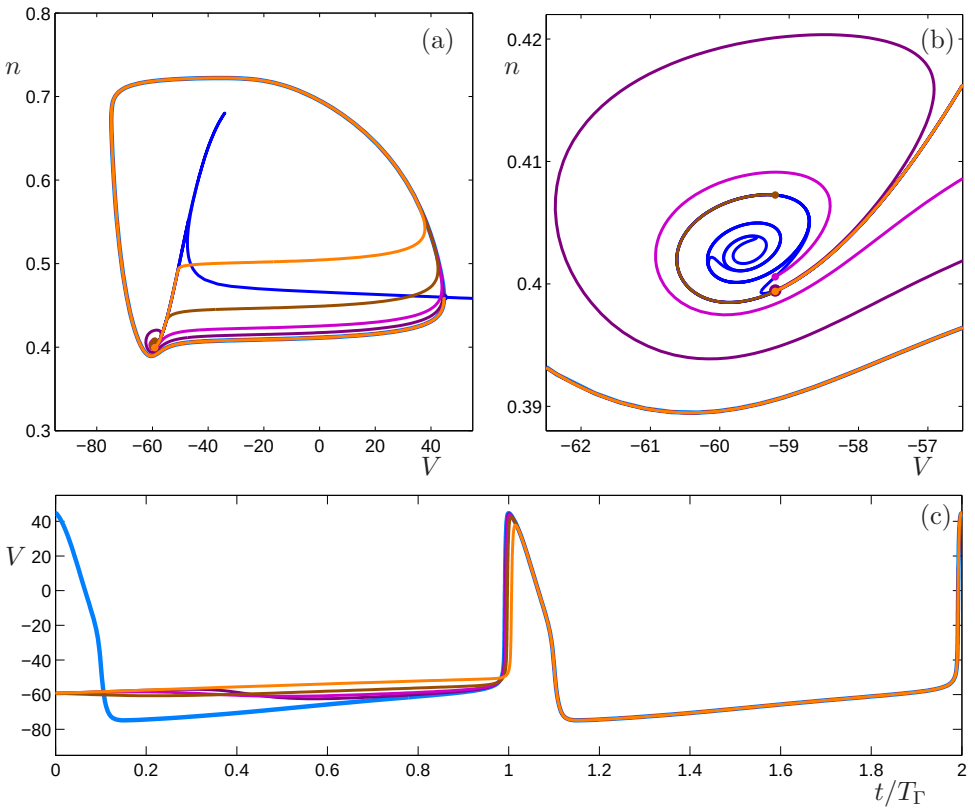

FIG. 6. *The transition from jump-left to jump-right orbits as the* 0*-phase isochron (dark blue) of the reduced Hodgkin-Huxley model* (4.1) *loops around the equilibrium. Four orbit segments are shown, each with* $V = -59.2$. *All four orbit segments lie on* $L_\eta(\gamma_0)$ *with* $\eta = 10^{-4}$ *after two periods. Panel (a) shows the phase plane, with an enlargement in panel (b); panel (c) shows the time series of* V *for these four orbit segments over two periods, overlaid on the corresponding time series for the periodic orbit (blue).*

ifold S^r_ε, or more precisely, $\mathbf{x}^r$, at a point that lies exactly one period T_Γ earlier on $\mathbf{x}^r$ than the intersection point of the first excursion of $\mathcal{I}(\gamma_0)$ with $\mathbf{x}^r$. We can deduce from Figure 6 that the transition from the second excursion to the third excursion of $\mathcal{I}(\gamma_0)$ will happen in much the same way as the transition illustrated in Figure 6 for the first excursion. Note that the second boomerang turn on $\mathcal{I}(\gamma_0)$, shown in Figure 6(b), is a rotated and contracted version of the first boomerang turn; similar transitions with similar further rotated and contracted boomerang turns happen for all subsequent excursions.

4.3. Properties of all global isochrons. The previous two sections described the behavior of the single isochron for the point γ_0 with zero phase, and the associated orbit segments. Any other point γ on the periodic orbit Γ of the reduced Hodgkin-Huxley model (4.1) will have a different isochron associated with a different phase $\theta(\gamma)$. However, the isochrons are a foliation of the stable manifold of Γ, which means that they are diffeomorphic transformations of $\mathcal{I}(\gamma_0)$. Indeed, if $\gamma = \Phi^{\theta T_\Gamma}(\gamma_0)$, then

$$\mathcal{I}(\Phi^{\theta T_\Gamma}(\gamma_0)) = \Phi^{\theta T_\Gamma}(\mathcal{I}(\gamma_0)).$$

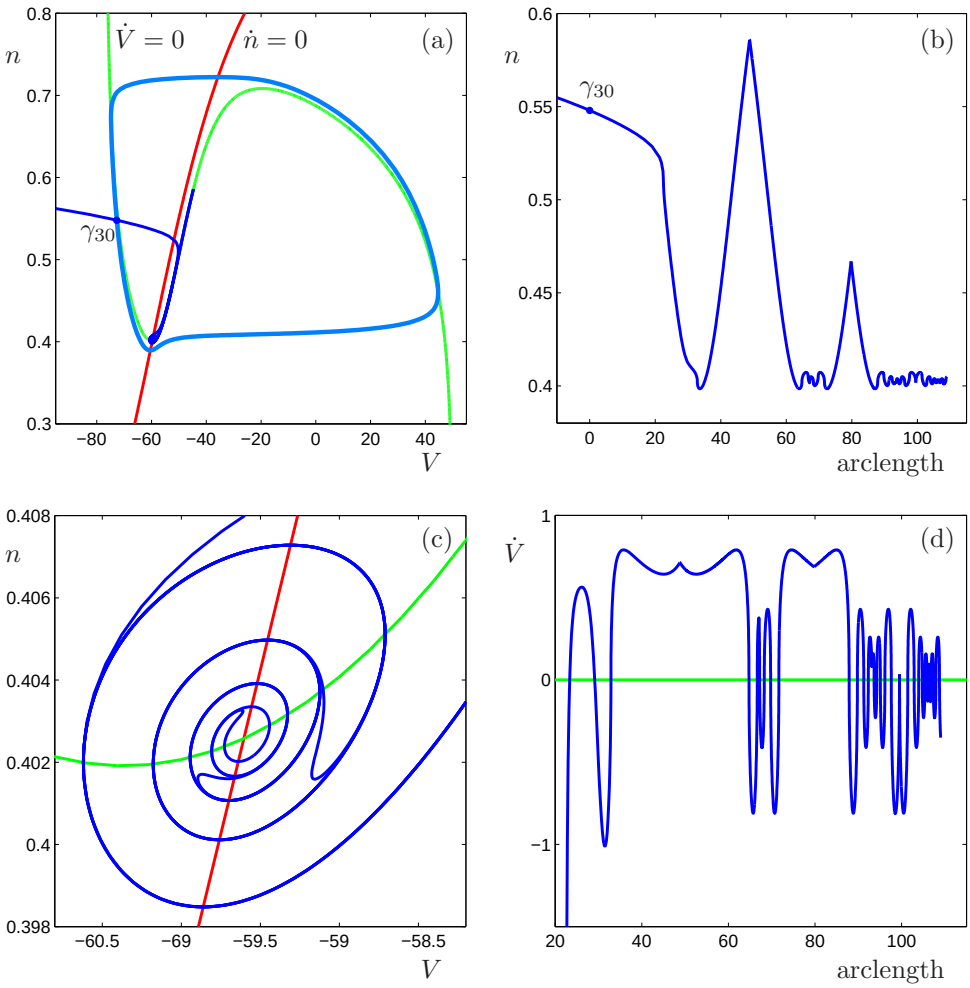

FIG. 7. *The isochron $\mathcal{I}(\gamma_{30})$ (dark blue) of the point γ_{30} with phase $\theta_{30}=\frac{30}{100}$ on the periodic orbit (blue) of the reduced Hodgkin-Huxley model* (4.1). *Panel (a) shows $\mathcal{I}(\gamma_{30})$ in the phase plane, along with the V-nullcline (green) and the n-nullcline (red); panel (b) shows the n-coordinate of $\mathcal{I}(\gamma_{30})$ versus its arclength; panel (c) is an enlargement to illustrate the accumulation onto the equilibrium $\mathbf{x}^*$ (not labeled); panel (d) shows the value of $\dot{V}$ along $\mathcal{I}(\gamma_{30})$ versus its arclength; compare also Figure 3. The associated animation* `anim-hhiso03.gif` *shows a point moving along the inside branch of $\mathcal{I}(\gamma_{30})$.*

In other words, $\mathcal{I}(\gamma)$ can be obtained by integrating each point on $\mathcal{I}(\gamma_0)$ for the fixed time $\theta\, T_\Gamma$, where $\theta=\theta(\gamma)$ is the phase of γ. Note that forward integration leads to a contraction towards Γ. Since $\mathcal{I}(\gamma_0)$ is computed up to a finite arclength, the transformation of $\mathcal{I}(\gamma_0)$ under the flow $\Phi^{\theta T_\Gamma}$ will lead to an approximation of $\mathcal{I}(\gamma)$ that has a shorter arclength. For θ close to 1, the shortening is $O(1)$ due to the large difference in time scales of the system.

We compute all isochrons $\mathcal{I}(\gamma)$ in the same way as $\mathcal{I}(\gamma_0)$, that is, we compute the stable manifold $W^{ss}(\gamma)$ as the invariant manifold of the time-T_Γ map that intersects the point γ on Γ. This means that the accuracy of $\mathcal{I}(\gamma)$ is the same as that of $\mathcal{I}(\gamma_0)$ and, in particular, we start with the linear approximation $L_\eta(\gamma)$ at

γ using the same bound $\eta = 10^{-4}$. Figure 7 shows an example of the isochron $\mathcal{I}(\gamma_{30})$ with $\gamma_{30} = \Phi^{\theta_{30}T_\Gamma}(\gamma_0)$, where $\theta_{30} = \frac{30}{100} = 0.3$; this means that $\gamma_{30} := (V, n) \approx (-72.7092, 0.5480)$, and the linear approximation is given by the direction $\vec{v}_{\gamma_{30}} := (-0.99999972, 0.00075031)$. As for $\mathcal{I}(\gamma_0)$, we perform continuation up to the time-$(4T_\Gamma)$ map. The figure is organized in the same way as Figure 3. Panel (a) shows $\mathcal{I}(\gamma_{30})$ in (V, n)-space along with the nullclines $\dot{V} = 0$ (green) and $\dot{n} = 0$ (red). The accompanying animation `anim-hhiso03.gif` illustrates how the inside branch of $\mathcal{I}(\gamma_{30})$ approaches the equilibrium $\mathbf{x}^*$ at the intersection of the two nullclines; see also the enlargement in panel (c). Figure 7(b) shows the n-coordinate of $\mathcal{I}(\gamma_{30})$ versus its arclength. The isochron first moves towards $\mathbf{x}^*$, but then it makes a counter-clockwise loop around $\mathbf{x}^*$ and starts making similar excursions as $\mathcal{I}(\gamma_0)$ that closely follow the V-nullcline, or more precisely, the slow manifold S^r_ε that lies exponentially close to the V-nullcline. The first two excursions are clearly seen in Figure 7(b); the first peak reaches $n \approx 0.5860$, which lies in between the peaks from the first ($n \approx 0.6802$) and second ($n \approx 0.5517$) excursions of $\mathcal{I}(\gamma_0)$, and the second peak reaches $n \approx 0.4669$. We observe in Figure 7(c) similar rotations around $\mathbf{x}^*$ and boomerang turns marking transitions from clockwise to counter-clockwise rotations as shown in Figure 3(c) for $\mathcal{I}(\gamma_0)$. Figure 7(d) shows the value of $\dot{V}$ versus the arclength of $\mathcal{I}(\gamma_{30})$. This figure also helps to understand the behavior, in particular near $\mathbf{x}^*$ in panel (c); below the V-nullcline in panel (c) we have $\dot{V} > 0$, and $\dot{V} < 0$ on the other side of the V-nullcline. Note that the first two crossings of the V-nullcline in Figure 7(d) happen at points on $\mathcal{I}(\gamma_{30})$ that lie before the points shown in Figure 7(c). That is, $\mathcal{I}(\gamma_{30})$ starts from γ_{30} in Figure 7(a) in the regime $\dot{V} < 0$ and it crosses the V-nullcline for a short arclength just before it enters a neighborhood of $\mathbf{x}^*$. The first counter-clockwise loop around $\mathbf{x}^*$ is the first downward peak in Figure 7(d) after about arclength 30 of $\mathcal{I}(\gamma_{30})$.

We calculated all one hundred isochrons $\mathcal{I}(\gamma_i)$ that are shown in Figure 2 in the same way; here $\gamma_i = \Phi^{\theta_i T_\Gamma}(\gamma_0)$, where $\theta_i = \frac{i}{100}$ for $i = 0, 1, \ldots, 99$. These isochrons all have properties similar to those for $\mathcal{I}(\gamma_0)$ and $\mathcal{I}(\gamma_{30})$, namely, apart from the initial approach to $\mathbf{x}^*$ each isochron makes a series of excursions followed by boomerang turns as it converges to $\mathbf{x}^*$.

4.4. Fundamental domains of isochrons. There clearly is a strong interaction between the isochrons of the reduced Hodgkin-Huxley model (4.1) and its repelling slow manifold S^r_ε. Each isochron makes a series of excursions that involve oscillations around S^r_ε. In this section we study this interaction in detail.

Let us focus again on the isochron $\mathcal{I}(\gamma_0)$ shown in Figure 3 and consider the location of the excursions of $\mathcal{I}(\gamma_{30})$, shown in Figure 7, relative to those of $\mathcal{I}(\gamma_0)$. As mentioned before, the first excursion of $\mathcal{I}(\gamma_{30})$ reaches a maximum $n \approx 0.5860$ that lies in between the maxima $n \approx 0.5517$ and $n \approx 0.6802$ of the second and first excursions of $\mathcal{I}(\gamma_0)$, respectively. Due to the steepness of the V-nullcline here, we can assume that the intersection points of $\mathcal{I}(\gamma_0)$ and $\mathcal{I}(\gamma_{30})$ with S^r_ε lie quite close to these maxima. Recall that S^r_ε is, in fact, a segment of the (special) orbit $\mathbf{x}^r = \mathbf{x}^r(t)$ that comes from $\mathbf{x}^*$. Let us denote the first three intersection points of $\mathcal{I}(\gamma_0)$ with $\mathbf{x}^r(t)$ by $\mathbf{r}_1$, $\mathbf{r}_2$ and $\mathbf{r}_3$, and let us assume that time along $\mathbf{x}^r(t)$ is chosen such that $\mathbf{r}_2 = \mathbf{x}^r(0)$. Then we have

$$\begin{aligned} \mathbf{r}_1 &= \mathbf{x}^r(T_\Gamma) &&= \Phi^{T_\Gamma}(\mathbf{r}_2) \quad \text{and} \\ \mathbf{r}_3 &= \mathbf{x}^r(-T_\Gamma) &&= \Phi^{-T_\Gamma}(\mathbf{r}_2). \end{aligned}$$

The first two intersection points of any isochron $\mathcal{I}(\gamma)$ with $\mathbf{x}^r(t)$ are then easily found using the phase $\theta(\gamma) = \theta$ of γ, namely, these are $\Phi^{\theta T_\Gamma}(\mathbf{r}_2)$ and $\Phi^{(\theta-1)T_\Gamma}(\mathbf{r}_2)$. Note

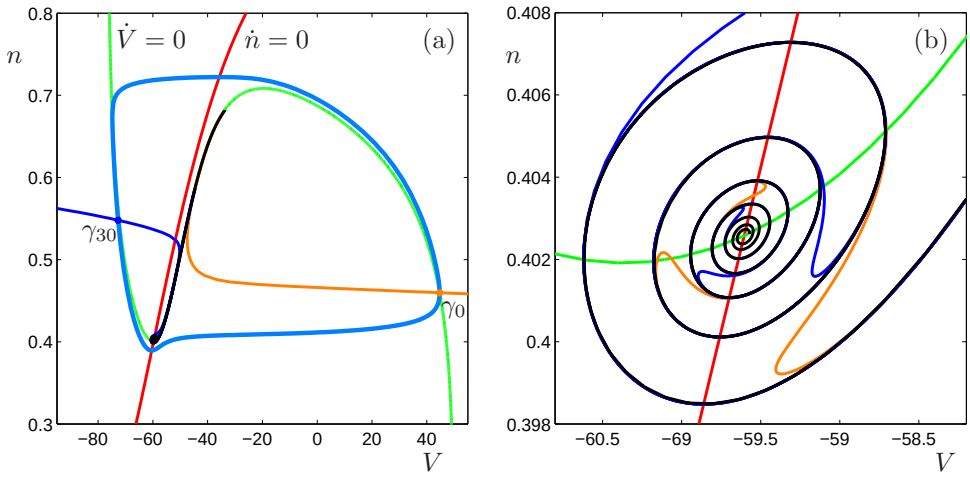

FIG. 8. *The isochrons $\mathcal{I}(\gamma_0)$ (orange) and $\mathcal{I}(\gamma_{30})$ (blue) of the reduced Hodgkin-Huxley equations* (4.1) *together with the orbit segment $\widehat{\mathbf{x}}^r$ (black) that contains the repelling slow manifold S^r_ε. Panel (a) shows the isochrons and $\widehat{\mathbf{x}}^r$ in the phase plane and panel (b) shows an enlargement near the equilibrium $\mathbf{x}^*$ (not labeled).*

that this holds for any $\theta \in [0,1]$. Hence, the segment between $\mathbf{x}^r(0)$ and $\mathbf{x}^r(T_\Gamma)$ defines a fundamental domain that consists of intersection points of *all* isochrons of Γ. Similarly, the segment between $\mathbf{x}^r(-T_\Gamma)$ and $\mathbf{x}^r(0)$ is such a fundamental domain, but now *all* isochrons of Γ will also pass this entire segment exponentially close twice in order to reach the first fundamental domain. In fact, we may define the entire orbit segment $\widehat{\mathbf{x}}^r := \{\mathbf{x}^r(t) \mid -\infty < t \leq 0\}$ as a curve along which *all* isochrons of Γ pass exponentially close at least twice.

Figure 8 shows both isochrons $\mathcal{I}(\gamma_0)$ and $\mathcal{I}(\gamma_{30})$ in one figure together with an approximation of $\widehat{\mathbf{x}}^r$ (black curve). The isochron $\mathcal{I}(\gamma_0)$ is colored orange and $\mathcal{I}(\gamma_{30})$ is colored dark blue, as before. The view in panel (a) shows that large parts of the two isochrons lie very close together virtually on top of $\widehat{\mathbf{x}}^r$. Indeed, even the enlargement in Figure 8(b) hardly distinguishes the curves; only the boomerang turns that correspond to transitions from clockwise to counter-clockwise rotations are different. Moreover, both isochrons make at least two excursions along $\widehat{\mathbf{x}}^r$ and the second excursion begins and ends (well) before the first (orange) boomerang turn of $\mathcal{I}(\gamma_0)$. Hence, what seems to be a single curve that leaves Figure 8(b) below the V-nullcline through the side $V = -58.2$ are, in fact, at least four curves, not counting $\widehat{\mathbf{x}}^r$. We can identify the segment just before the first (orange) boomerang turn of $\mathcal{I}(\gamma_0)$ (which corresponds to the end of its first excursion) and the segment immediately after the first clockwise rotation of $\mathcal{I}(\gamma_0)$ around $\mathbf{x}^*$ (which corresponds to the start of its second excursion) as marking a strip that contains all these curves.

We can give similar arguments for any isochron $\mathcal{I}(\gamma)$ with phase $\theta(\gamma) = \theta$. Indeed, this isochron must reach the point $\Phi^{(\theta-1)T_\Gamma}(\mathbf{r}_2)$, associated with its phase θ, that lies in between $\mathbf{r}_3$ and $\mathbf{r}_2$ on $\widehat{\mathbf{x}}^r$. Moreover, in doing so it cannot intersect another isochron. Therefore, *all* isochrons must pass through the strip bounded by the first and second excursions of $\mathcal{I}(\gamma_0)$. This means that the seemingly single curve that leaves Figure 8(b) below the V-nullcline through the side $V = -58.2$ consist of infinitely many curves!

Figure 9 presents a different illustration of the phenomenon. Shown are two

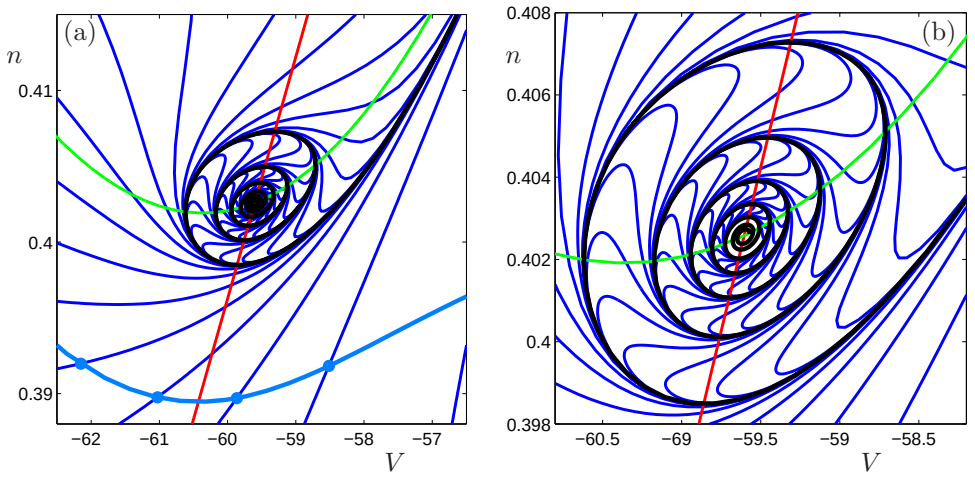

FIG. 9. *A total of 20 isochrons (dark blue) uniformly distributed in time along the stable periodic orbit (blue) of the reduced Hodgkin-Huxley model* (4.1). *Shown are two successive enlargements near the equilibrium* $\mathbf{x}^*$ *(not labeled). The black curve represents the orbit segment* $\widehat{\mathbf{x}}^r$.

successive enlargements near the equilibrium $\mathbf{x}^*$ of Figure 2, where we plot only twenty isochrons, that is, every fifth isochron in Figure 2. The approximation of $\widehat{\mathbf{x}}^r$ (black curve) is overlaid in both panels. We observe a self-similar structure of the isochrons in this neighborhood of $\mathbf{x}^*$, and the foliation of the phase space by the isochrons appears to be organized by a contracting transformation that is reminiscent of a λ-lemma [37]; certainly, the successive points $\Phi^{-kT_\Gamma}(\mathbf{r}_2)$ contract to $\mathbf{x}^*$ in accordance with the λ-lemma.

Winfree conjectures in [43, Conjecture C in the Appendix] that any isochron must come arbitrarily close to any point in the phaseless set, that is, the boundary $\partial\mathcal{B}$ of the basin of attraction $\mathcal{B}(\Gamma)$ of Γ. For our example, this means that all isochrons come arbitrarily close to the equilibrium $\mathbf{x}^*$, which is the only point in the phaseless set. Figure 8 illustrates that $\widehat{\mathbf{x}}^r$, which lies in the *interior* of $\mathcal{B}(\Gamma)$ is an 'almost phaseless set,' because all isochrons come exponentially close to $\widehat{\mathbf{x}}^r$, rather than arbitrarily close. Our findings do not contradict Winfree's conjecture, but they do show that extreme phase sensitivity can occur on a codimension-one set in the interior of $\mathcal{B}(\Gamma)$.

To be more precise, while all isochrons are exponentially close to (the left of) the segment on $\widehat{\mathbf{x}}^r$ in between $\mathbf{x}^r(0)$ and $\mathbf{x}^r(T_\Gamma)$, they are even closer (on both sides) to the segment in between $\mathbf{x}^r(-T_\Gamma)$ and $\mathbf{x}^r(0)$, and again even closer to the segment in between $\mathbf{x}^r(-2T_\Gamma)$ and $\mathbf{x}^r(-T_\Gamma)$, and so on. Of course, these segments on $\widehat{\mathbf{x}}^r$ in between $\mathbf{x}^r(-kT_\Gamma)$ and $\mathbf{x}^r(-(k-1)T_\Gamma)$ for $k = 1, 2, \ldots$, become successively shorter and lie successively closer to $\mathbf{x}^*$. However, the arclength of the segment in between $\mathbf{x}^r(-T_\Gamma)$ and $\mathbf{x}^r(0)$ decreases with the ratio ε of the slow and fast time scales and is zero in the limit $\varepsilon \to 0$. Note that a change in the ratio between two time scales alters the slow manifold S^r_ε — it lies closer to the V-nullcline as ε decreases. For each ε we can define a corresponding orbit segment $\mathbf{x}^r_\varepsilon(t)$ such that $\mathbf{x}^r_\varepsilon(0)$ is equal to the second intersection of $\mathcal{I}(\gamma_0)$ with $\mathbf{x}^r_\varepsilon(t)$. It is important to realize that the first intersection of $\mathcal{I}(\gamma_0)$ with $\mathbf{x}^r_\varepsilon(t)$ will always be well away from $\mathbf{x}^*$; in fact, this point will move further away in arclength along $\mathbf{x}^r_\varepsilon(t)$, rather than closer to $\mathbf{x}^*$ as ε decreases. If we consider an ε-dependent family of the reduced Hodgkin-Huxley equation, then for arbitrary

distance ρ and arbitrary $k \in \mathbb{N}$, we can choose $0 < \varepsilon \ll 1$ such that all isochrons will pass within distance ρ of any point on the segment $\{\mathbf{x}_\varepsilon^r(t) \mid -\infty < t \leq -kT_\Gamma\}$.

5. Discussion. We have presented a numerical method for the computation of global isochrons in planar systems. It is based on two-point boundary value continuation and implemented in the latest version of AUTO [11]. We compute a global isochron $\mathcal{I}(\gamma)$ as the global stable manifold of the fixed point γ of the time-T_Γ map, where T_Γ is the period of the underlying periodic orbit. Based on the method in [15], we view the isochron as a one-parameter family of orbit segments with one end point on the approximation computed so far, and the other tracing new parts of the global manifold. Each continuation step uses global information about the variation along the entire orbit segment to control the accuracy of the computation. Hence, the extreme sensitivity of initial conditions that is typical for slow-fast systems is spread effectively along the entire orbit segment. Furthermore, the adaptive step selection of AUTO ensures that the continuation generates a nicely distributed mesh along each isochron that automatically parameterizes the curves by arclength. The Python scripting interface of AUTO [11] allows one to select and compute automatically an arbitrary number of isochrons along a periodic orbit that are uniformly spaced in time or arclength. The numerical accuracy and convergence properties of this approach allow the computation of one-dimensional isochrons up to unprecedented arclengths.

We illustrated the algorithm with the example of a reduced Hodgkin-Huxley model that was considered in [28, 34]. We found that the isochrons of this planar slow-fast system are organized in a remarkably complex structure, a phenomenon that we believe is not specific to this example. As predicted by the theory [21, 43], the isochrons foliate the plane, with one side extending to infinity and the other converging to the sole singularity at the equilibrium $\mathbf{x}^*$ of the reduced Hodgkin-Huxley model. However, the convergence to this phaseless set is by no means immediate. The isochrons make several 'excursions' along the repelling slow manifold of the reduced Hodgkin-Huxley model. During each such excursion, the isochron passes both to the left and the right of the repelling slow manifold, corresponding to trajectories that converge to the periodic orbit via a left or right jump along the fast direction of the system, respectively.

The geometry of the isochrons in a neighborhood of the equilibrium $\mathbf{x}^*$ for the reduced Hodgkin-Huxley model nicely illustrates the extreme phase sensitivity that exists in the neighborhood of a phaseless set. Such sensitivity was postulated by Winfree [43], who noted that a system near a phaseless set could have its phase randomized by small noise, an idea which has been applied, for example, in [8] to desynchronize a population of neurons; in particular, the phase of each neuron is altered randomly after the system is driven to the phaseless set using minimal-time optimal control with an amplitude-constrained input current. Winfree also considered the case where the attracting periodic orbit is not a global attractor and its basin has a one-dimensional boundary $\partial\mathcal{B}$. This boundary is also a phaseless set and the phase sensitivity in a neighborhood of $\partial\mathcal{B}$ is also extreme in the sense that all isochrons come arbitrarily close to $\partial\mathcal{B}$.

We found that the neighborhood of the repelling slow manifold for the reduced Hodgkin-Huxley model is also a region of phase space which will display phase sensitivity, even though it is not a true phaseless set. Indeed, our calculations illustrate that the isochrons concentrate near the repelling slow manifold, which is why we call it an 'almost phaseless set.' (We note that, in the limit $\varepsilon \to 0$ of the ratio $\varepsilon \ll 1$ between the slow and fast time scales of the system, the repelling slow manifold con-

verges to a phaseless set.) This suggests that a controller such as that considered in [8] could target the repelling slow manifold rather than the equilibrium $\mathbf{x}^*$ in order to desynchronize a population of neurons through phase randomization.

In theory, it is straightforward to generalize the computational method presented in this paper to isochrons of three- or higher-dimensional vector fields. However, the isochrons are then two- or higher-dimensional manifolds and their computation becomes increasingly difficult for the same reasons as the computation of global two- or higher-dimensional stable manifolds [31].

Acknowledgments. We are grateful to Bernd Krauskopf for his careful reading of a first draft of this manuscript, and to Jakub Nowacki for pointing out the use of isochrons in the control and synchronization of power systems. We thank John Guckenheimer and Erik Sherwood for helpful discussions. JM acknowledges the support and hospitality of the University of Bristol during his visit that started this project. HMO acknowledges the support and hospitality of Cornell University, where part of this work was carried out.

REFERENCES

[1] É. Benoît, J. L. Callot, F. Diener, and M. Diener, *Chasse au canards*, Collect. Math., 31 (1981), pp. 37–119.

[2] E. Brown, P. Holmes, and J. Moehlis, *Globally coupled oscillator networks*, in Perspectives and Problems in Nonlinear Science: A Celebratory Volume in Honor of Larry Sirovich, E. Kaplan, J. Marsden, and K. Sreenivasan, eds., Springer-Verlag, New York, 2003, pp. 183–215.

[3] E. Brown, J. Moehlis, and P. Holmes, *On the phase reduction and response dynamics of neural oscillator populations*, Neural Comp., 16 (2004), pp. 673–715.

[4] X. Cabré, E. Fontich and R. de la Llave, *The parameterization method for invariant manifolds. III: Overview and applications*, J. Differential Equations, 218 (2005), pp. 444–515.

[5] A. Campbell, A. Gonzalez, D. L. Gonzalez, O. Piro and H. A.Larrondo, *Isochrones and the dynamics of kicked oscillators*, Phys. A, 155 (1989), pp. 565–584.

[6] P. Danzl, R. Hansen, G. Bonnet, and J. Moehlis, *Partial phase synchronization due to random Poisson inputs*, J. Comp. Neurosci., 25 (2008), pp. 141-157.

[7] P. Danzl and J. Moehlis, *Spike timing control of oscillatory neurons using impulsive and quasi-impulsive charge-balanced inputs*, in Proceedings of the 2008 American Control Conference, 2008, pp. 171-176.

[8] P. Danzl, J. Hespanha, and J. Moehlis, *Event-based minimum-time control of oscillatory neuron models: phase randomization, maximal spike rate increase, and desynchronization*, Biol. Cybernetics, in press.

[9] V. De Witte and W. Govaerts, *Convergence analysis of a numerical method to solve the adjoint equations*, preprint Ghent University, 2009.

[10] E. J. Doedel, *Lecture notes on numerical analysis of nonlinear equations*, in Numerical Continuation Methods for Dynamical Systems: Path following and boundary value problems, B. Krauskopf, H. M. Osinga, and J. Galán-Vioque, eds., Springer-Verlag, New-York, 2007, pp. 1–50.

[11] E. J. Doedel, AUTO-07P*: Continuation and bifurcation software for ordinary differential equations*, with major contributions by A. R. Champneys, F. Dercole, T. F. Fairgrieve, Yu. A. Kuznetsov, B. E. Oldeman, R. C. Paffenroth, B. Sandstede, X. J. Wang and C. Zhang; available via `http://cmvl.cs.concordia.ca/auto/`.

[12] E. J. Doedel, B. W. Kooi, G. A. K. van Voorn, Yu. A. Kuznetsov, *Continuation of connecting orbits in 3D-ODEs (I): Point-to-cycle connections*, Int. J. Bif. Chaos, 18(7) (2008), pp. 1889–1903.

[13] E. J. Doedel, B. W. Kooi, G. A. K. van Voorn, Yu. A. Kuznetsov, *Continuation of connecting orbits in 3D-ODEs (II): Cycle-to-cycle connections*, Int. J. Bif. Chaos, 19(1) (2009), pp. 159–169.

[14] F. Dumortier and R. Roussarie, *Canard cycles and center manifolds*, Mem. Amer. Math. Soc., 121(577) (1996).

[15] J. P. England, B. Krauskopf, and H. M. Osinga, *Computing one-dimensional global manifolds of Poincaré maps by continuation*, SIAM J. Applied Dynamical Systems, 4(4) (2005), pp. 1008–1041.
[16] G. B. Ermentrout, *Simulating, Analyzing, and Animating Dynamical Systems: A Guide to XPPAUT for Researchers and Students*, SIAM, Philadelphia, 2002.
[17] G. B. Ermentrout and N. Kopell, *Multiple pulse interactions and averaging in coupled neural oscillators*, J. Math. Biol., 29 (1991), pp. 195–217.
[18] L. Glass and M. C. Mackey, *From Clocks to Chaos: The Rhythms of Life*, Princeton University Press, Princeton, 1988.
[19] W. Govaerts and B. Sautois, *Computation of the phase response curve: A direct numerical approach*, Neural Comp., 18 (2006), pp. 817–847.
[20] A. J. Grono, J. J. Wlodarski, *Setting and testing automatic generator synchronizers*, IEEE Computer Applications in Power, 12(1) (1999), pp. 38–40.
[21] J. Guckenheimer, *Isochrons and phaseless sets*, J. Math. Biol., 1 (1975), pp. 259–273.
[22] A. Guillamon and G. Huguet, *A computational and geometric approach to phase resetting curves and surfaces*, SIAM J. Appl. Dyn. Sys., 8(3) (2009), pp. 1005–1042.
[23] B. S. Gutkin, G. B. Ermentrout, and A. D. Reyes, *Phase-response curves give the responses of neurons to transient inputs*, J. Neurophysiol., 94 (2005), pp. 1623–1635.
[24] M. W. Hirsch, C. C. Pugh, and M. Shub, *Invariant Manifolds*, Vol. **583** of Lecture Notes in Math., Springer-Verlag, New-York, 1977.
[25] A. L. Hodgkin and A. F. Huxley, *A quantitative description of membrane current and its application to conduction and excitation in nerve*, J. Physiol., 117 (1952), pp. 500–544.
[26] F. C. Hoppensteadt and E. M. Izhikevich, *Weakly Connected Neural Networks*, Springer-Verlag, New York, 1997.
[27] E. M. Izhikevich, *Dynamical Systems in Neuroscience: The Geometry of Excitability and Bursting*, MIT Press, Cambridge, Massachusetts, 2007.
[28] J. Keener and J. Sneyd, *Mathematical Physiology*, Springer-Verlag, New York, 1998.
[29] B. Krauskopf and H. M. Osinga, *Growing 1D and quasi 2D unstable manifolds of maps*, J. Comput. Phys., 146(1) (1998), pp. 404–419.
[30] B. Krauskopf and H. M. Osinga, *Computing invariant manifolds via the continuation of orbit segments*, in Numerical Continuation Methods for Dynamical Systems: Path following and boundary value problems, B. Krauskopf, H. M. Osinga, and J. Galán-Vioque, eds., Springer-Verlag, New-York, 2007, pp. 117–154.
[31] B. Krauskopf, H. M. Osinga, E. J. Doedel, M. E. Henderson, J. Guckenheimer, A. Vladimirsky, M. Dellnitz, and O. Junge, *A survey of methods for computing (un)stable manifolds of vector fields*, Internat. J. Bifur. Chaos Appl. Sci. Engrg., 15(3) (2005), pp. 763–791.
[32] B. Krauskopf and T. Riess, *A Lin's method approach to finding and continuing heteroclinic connections involving periodic orbits*, Nonlinearity, 21(8) (2008), pp. 1655–1690.
[33] Y. Kuramoto, *Chemical Oscillations, Waves, and Turbulence*, Springer-Verlag, Berlin, 1984.
[34] J. Moehlis, *Canards for a reduction of the Hodgkin-Huxley equations*, J. Math. Biol., 52 (2006), pp. 141–153.
[35] J. Moehlis, E. Shea-Brown, and H. Rabitz, *Optimal inputs for phase models of spiking neurons*, ASME J. Comp. Nonlin. Dyn., 1 (2006), pp. 358-367.
[36] H. M. Osinga and G. R. Rokni Lamooki, *Numerical study of manifold computations*, in Proceedings of the International Conference on Differential Equations, F. Dumortier, H. W. Broer, J. Mawhin, A. Vanderbauwhede, and S. Verduyn Lunel, eds., Equadiff 2003, Hasselt, World Scientific, Singapore, 2005, pp. 190–195.
[37] J. Palis and W. De Melo, *Geometric Theory of Dynamical Systems*, Springer-Verlag, Berlin, 1982.
[38] T. Pavlidis, *Biological Oscillators: Their Mathematical Analysis*, Academic Press, New York, 1973.
[39] W. E. Sherwood, *Phase Response in Networks of Bursting Neurons: Modeling Central Pattern Generators*, PhD thesis from Cornell University, January 2008.
[40] W. M. Strang, C. J. Mozina, B. Beckwith, T. R. Beckwith, S. Chhak, E. C. Fennell, E. W. Kalkstein, K. C. Kozminski, A. .C. Pierce, P. W. Powell, D. W. Smaha, J. T. Uchiyama, S. M. Usman, and W. P. Waudby, *Generator synchronizing industry survey results*, IEEE Trans. Power Delivery, 11(1) (1996), pp. 174–183.
[41] S. H. Strogatz, *From Kuramoto to Crawford: exploring the onset of synchronization in populations of coupled oscillators*, Physica D, 143 (2000), pp. 1–20.
[42] A. Timbus, R. Teodorescu, F. Blaabjerg, and M. Liserre, *Synchronization methods for three phase distributed power generation systems. An overview and evaluation*, IEEE 36th

Power Electronics Specialists Conference, PESC '05, (2005), pp. 2474–2481.
[43] A. T. Winfree, *Patterns of phase compromise in biological cycles*, J. Math. Biol., 1(1) (1974), pp. 73–93
[44] A. T. Winfree, *The Geometry of Biological Time, Second Edition*, Springer-Verlag, New York, 2001.